

Spontaneous emission rate and the density of states inside a one dimensional photonic crystal

Ebrahim Forati, *Member, IEEE*

Abstract—Different densities of electromagnetic states inside a one dimensional photonic crystal (1D PC) are studied. Hertz vector formalism is used to calculate Green's tensor inside a layered structure, semi-analytically. Based on the obtained Green's tensor, the local density of electromagnetic states (LDOS) and the density of states (DOS) inside a 1D PC are calculated and discussed. The Green's tensor is also used to approximate the density of Bloch states inside the 1D PC and is compared with its exact calculation based on the 1D PC dispersion relations. Using a practical 1D PC parameters in the visible range, the aforementioned quantities are calculated and verified with a full-wave solver based on finite element method (FEM). The formulations and the results are aimed to be helpful in thermal and spontaneous radiation studies.

Index Terms—Density of electromagnetic states, photonic crystal, Green's function.

I. INTRODUCTION

THE density of electromagnetic modes/states (DOS) in a homogeneous isotropic medium is defined as the number of available electromagnetic modes per volume per frequency. It is an important quantity in statistical physics including thermal energy radiation where the degeneracy of the energy levels (related to the photons' frequencies) is a determining parameter in the thermodynamical arguments. The DOS is often used as the degeneracy function in such thermal radiation studies. A well-known example is the conventional broadband thermal radiation which obeys Planck's blackbody radiation [1], [2] (i.e. radiations from Sun, a tungsten light bulb, etc.) The DOS also has significant importance in quantum electrodynamics (QED) where physics of spontaneous emission, vacuum fluctuations, Van der Waals and Casimir forces, etc. depend on the environment DOS. Note, the DOS in this work refers to the photonic states. The term is also used for the density of available electronic states in solid state physics.

A closely related parameter to the DOS is the local density of electromagnetic states (LDOS) which is defined to be proportional to the energy released by a unity dipole transition (point current source) per second. The released energy travels away from the source as photons. For a point current source at \mathbf{r}_0 , radial frequency of ω , and in the direction of $\hat{\alpha}$, $\mathbf{J}(\mathbf{r}', \omega') = \hat{\alpha} \delta(\mathbf{r}' - \mathbf{r}_0) \delta(\omega' - \omega)$, the LDOS is

$$\text{LDOS}(\mathbf{r}_0, \omega, \hat{\alpha}) = \frac{12\varepsilon_0\varepsilon_r}{\pi} \text{P}(\mathbf{r}_0, \omega, \hat{\alpha}) \quad (1)$$

where $\text{P}(\mathbf{r}_0, \omega, \hat{\alpha}) = \frac{1}{2} \text{Re} \{ \mathbf{E}(\mathbf{r}_0, \omega) \cdot \mathbf{J}(\mathbf{r}_0, \omega) \}$ is the power released by $\mathbf{J}(\mathbf{r}_0, \omega)$, and ε_r is the relative permittivity of the medium (ε_0 and μ_0 are the free space permittivity and

permeability, respectively.) It is common to express (1) in terms of the dyadic Green's tensor as [3]

$$\text{LDOS}(\mathbf{r}_0, \omega, \hat{\alpha}) = \frac{6\omega\mu_r\varepsilon_r}{\pi c^2} \left| \text{Im} \left(\hat{\alpha} \cdot \overline{\overline{\mathbf{G}}}(\mathbf{r}_0, \mathbf{r}_0, \omega) \cdot \hat{\alpha} \right) \right|, \quad (2)$$

where the Green's tensor, in an isotropic medium, satisfies

$$\nabla \times \nabla \times \overline{\overline{\mathbf{G}}}(\mathbf{r}_0, \mathbf{r}', \omega) - k_0^2 \mu_r \varepsilon_r \overline{\overline{\mathbf{G}}}(\mathbf{r}_0, \mathbf{r}', \omega) = \delta(\mathbf{r}_0 - \mathbf{r}') \overline{\overline{\mathbf{I}}}, \quad (3)$$

in which $k_0 = \omega \sqrt{\varepsilon_0 \mu_0}$ is the free space wavenumber, $\overline{\overline{\mathbf{I}}}$ is the dyadic unity matrix, μ_r is the relative permeability of the medium at the source location, and c is the speed of light in free space. We use $e^{j\omega t}$ time harmonic convention throughout the paper, and the primed notation is used for the source parameters. The electric field is related to the Green's tensor as

$$\mathbf{E}(\mathbf{r}, \omega) = j\omega\mu_0\mu_r \int_{\mathbf{r}'} \overline{\overline{\mathbf{G}}}(\mathbf{r}, \mathbf{r}', \omega) \cdot \mathbf{J}(\mathbf{r}', \omega) d\mathbf{r}'. \quad (4)$$

It is straight forward to convert (1) to (2) since $\hat{\alpha} \cdot \mathbf{E}(\mathbf{r}_0, \omega) = j\omega\mu_0\mu_r \left(\hat{\alpha} \cdot \overline{\overline{\mathbf{G}}}(\mathbf{r}_0, \mathbf{r}_0, \omega) \cdot \hat{\alpha} \right)$.

Note, we also assumed that, for our purpose, the medium's responses to an electric and a magnetic point sources are similar, hence the LDOS can be calculated by only considering an electric point source. In general, (2) should be written as [4]

$$\text{LDOS}(\mathbf{r}_0, \omega, \hat{\alpha}) = \frac{3\omega\mu_r\varepsilon_r}{\pi c^2} \left(\left| \text{Im} \left(\hat{\alpha} \cdot \overline{\overline{\mathbf{G}}}_{\mathbf{E}}(\mathbf{r}_0, \mathbf{r}_0, \omega) \cdot \hat{\alpha} \right) \right| + \left| \text{Im} \left(\hat{\alpha} \cdot \overline{\overline{\mathbf{G}}}_{\mathbf{H}}(\mathbf{r}_0, \mathbf{r}_0, \omega) \cdot \hat{\alpha} \right) \right| \right) \quad (5)$$

where both $\overline{\overline{\mathbf{G}}}_{\mathbf{E}}(\mathbf{r}_0, \mathbf{r}_0, \omega)$ and $\overline{\overline{\mathbf{G}}}_{\mathbf{H}}(\mathbf{r}_0, \mathbf{r}_0, \omega)$ satisfy (3), and $\hat{\alpha} \cdot \mathbf{H}(\mathbf{r}_0, \omega) = j\omega\varepsilon_0\varepsilon_r \left(\hat{\alpha} \cdot \overline{\overline{\mathbf{G}}}_{\mathbf{H}}(\mathbf{r}_0, \mathbf{r}_0, \omega) \cdot \hat{\alpha} \right)$. To keep the formulations simpler, we continue with (3) throughout the rest of this paper. The effect of this approximation on the final results will be discussed later.

LDOS is a critical parameter in nano-photonics and quantum optics [5]–[7]. In particular, the spontaneous emission rate of an emitter in a medium is proportional to the LDOS via Fermi's golden rule. As a known example, the spontaneous emission prohibition in photonics crystals (PC) is achieved by engineering LDOS=0 around the transition frequency of the emitters [8]–[12]. Unlike DOS, the LDOS has both location and direction dependences, as well as its implicit dependence on the density of available states and their couplings to the

source. In a homogeneous isotropic medium, DOS and LDOS are essentially the same.

Although DOS can only be defined, accurately, in a homogeneous isotropic material, we may estimate it in a periodic structure using the LDOS as [13]

$$\text{DOS}(\omega) = \frac{1}{V} \int_V \frac{1}{3} \text{Tr}(\text{LDOS}(\mathbf{r}, \omega, \hat{\alpha})) d\mathbf{r}, \quad (6)$$

where V is the volume of the unit cell in the periodic structure, and the $\frac{1}{3} \text{Tr}(\cdot)$ operator takes the average on the three spatial orthonormal directions.

The estimated DOS of a photonic crystal (PC) is of particular interest as its thermal emission is argued to surpass Planck's limit [7], [14], [15]. In fact, there are experimental evidences of emission beyond Planck's limit by PCs (as high as 100 times) around their band edges [16]. One of the most recent experimental confirmations is reported in [17] where emission from a tungsten PC and a blackbody sample are compared under the same conditions. They observed sharp emission peaks from the PC (relative to the blackbody), similar to those in DOS of an unbounded PC. However, finding DOS inside a semi-infinite PC (emitting into the free half-space above it) needs a careful treatment, as the electromagnetic modes of the two half-spaces are different and only partially coupled. In fact, there are wave-guided modes inside a 1D PC which cannot couple to the outside environment. Examples of such analysis are [14], [18], [19] only some of which support the possibility of thermal emission beyond Planck's limit.

The accurate calculation of the LDOS including its polarization dependence (and its consequent DOS) inside a 1D PC is a challenging mathematical problem. Several studies have considered the on-axis modes (plane waves traveling perpendicular to the 1D PC boundaries) densities, which have band-gaps and lead to sharp peaks in the calculated LDOS [20], [21]. However, the total LDOS of a 1D PC does not have any band-gap [22] and the term LDOS in such works should be inferred as the local density of on-axis states. The LDOS calculations in [23] also uses Green's functions with some approximations (called Local Perturbation Method) and ignores the source's polarization (Green's function instead of Green's tensor). In [24], [25], dielectric slabs are modeled with infinitely thin plane scatterers, and a multiple scattering formalism is set up to calculate the LDOS. The polarization dependence of the LDOS is preserved in this formulation, but a simplified model (i.e. an array of infinitely thin plane scatterers) is used instead of the 1D PC.

In [26], Hertz vector formalism is used to formulate the exact Green's tensor inside a layered structure (the exact formulation is also derived for a single slab in [27]). The integrations required in the Green's tensor calculation (for inverse Fourier transforms) are also solved analytically using the complex plane analysis (as Sommerfeld did, see [28], [29]) and mapping techniques such as finding the steepest descent path. This calculation is exact, but it includes reflection coefficients from the stacks above and below the source layer (viz. the layer hosting the point source) as well as the transmission coefficients from the source layer to the outermost layers.

This is great for when the reflection/transmission coefficients calculations are convenient (e.g. thin film stacks, mirrors, etc.) However, finding the reflection/transmission coefficients is a separate problem and is not necessarily an easy task. The same argument applies to [30].

In this paper, Hertz vector formalism is used to formulate Green's tensor inside a layered structure in a matrix form, which is then solved numerically to find Hertz vectors in all the layers. The advantage of this formulation is that no reflection/transmission coefficients are needed to be calculated separately. Also, the integrations are solved numerically by adding a small loss to the structure (to avoid singularities). The formulation is intended to be more convenient for scripting and to be easily scalable for High Performance Computing (HPC).

In the followings, first the exact dyadic Green's tensor of a layered structure are formulated. Next, LDOS and DOS inside a 1D PC are calculated. We will also discuss the calculation of the density of Bloch modes using our layered media approach, as well as its exact calculation based on the 1D PC dispersion relations. Using a practical 1D PC example, these different mode densities are calculated and compared. The results are also compared with the numerical calculations based on finite element method (FEM). The implications of the results to thermal emission by a 1D PC will also be discussed briefly.

LDOS AND DOS INSIDE A 1D PC

We start by the Green's tensor expression (using Fourier transform) inside a layered structure shown in Fig. 1

The first and last layers are infinitely large in x -direction, the source is at the origin inside the m th layer, and the boundaries are at $x = d_{1,2,\dots,(N-1)}$. Defining two dimensional spatial Fourier transform pair as

$$f(x, y, z) = \frac{1}{(2\pi)^2} \iint_{-\infty}^{\infty} F(x, q_y, q_z) e^{j(q_y y + q_z z)} dq_y dq_z, \quad (7)$$

$$F(x, q_y, q_z) = \iint_{-\infty}^{\infty} f(x, y, z) e^{-j(q_y y + q_z z)} dy dz, \quad (8)$$

we may write the n th layer's wave equation in terms of the Hertzian dipole, $\pi_{\mathbf{n}} = \pi_{\mathbf{n}}^x \hat{x} + \pi_{\mathbf{n}}^y \hat{y} + \pi_{\mathbf{n}}^z \hat{z}$, in Fourier transform domain as [31], [32]

$$\left(\frac{\partial^2}{\partial x^2} - p_n^2 \right) \pi_{\mathbf{n}}(x, q_y, q_z) = -\frac{1}{j\omega\epsilon_0\epsilon_n} \mathbf{J}(x, q_y, q_z) \delta^{Kron}(n-m) \quad (9)$$

where $\delta^{Kron}(\cdot)$ is the Kronecker delta function, and $p_n = \sqrt{q_y^2 + q_z^2 - k_0^2 \mu_n \epsilon_n}$, and the layer m contains the source. Without loss of generality, we assume the current is zero in z -direction ($\mathbf{J} = J^x \hat{x} + J^y \hat{y}$), which also turns out to give $\pi_{\mathbf{n}}^z = 0$. The solution to (9) is [31]–[35]

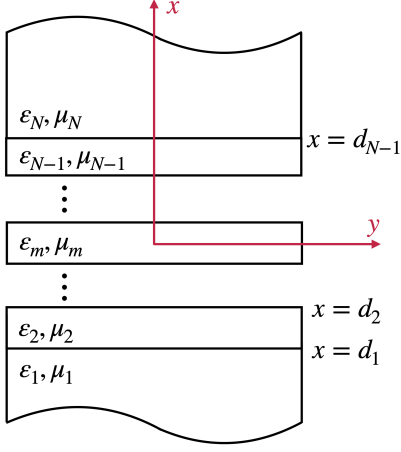


Fig. 1. A one dimensional layered structure. The point source is at the origin inside layer m (i.e. the coordinate system moves according to the source location). Layers 1 and N in x -direction, and all layers in y - and z - directions, are infinitely large. ϵ and μ are relative permittivity and permeability of the layers, respectively.

$$\begin{aligned} \pi_n^i(x, q_y, q_z) = & A_n^i e^{-p_n x} + B_n^i e^{p_n x} \\ & + \delta^{Kron}(n-m) \int_{-\infty}^{\infty} \frac{e^{-p_n |x-x'|} J^i(x')}{2p_n j\omega\epsilon_0\epsilon_n} dx', \end{aligned} \quad (10)$$

where $i = x, y$, and A_n^i, B_n^i are the unknown coefficients to be determined from the boundary conditions.

The electric and magnetic fields are related to the Hertzian dipoles, in the matrix form, as

$$\mathbf{E}_n(x, q_y, q_z) = \begin{bmatrix} \hat{x} & \hat{y} & \hat{z} \end{bmatrix} \begin{bmatrix} k_0^2 \mu_n \epsilon_n + \frac{\partial^2}{\partial x^2} & j q_y \frac{\partial}{\partial x} & \\ j q_y \frac{\partial}{\partial x} & k_0^2 \mu_n \epsilon_n - q_y^2 & \\ j q_z \frac{\partial}{\partial x} & -q_y q_z & \end{bmatrix} \begin{bmatrix} \pi_n^x \\ \pi_n^y \end{bmatrix}, \quad (11)$$

$$\mathbf{H}_n(x, q_y, q_z) = j\omega\epsilon_0\epsilon_n \begin{bmatrix} \hat{x} & \hat{y} & \hat{z} \end{bmatrix} \begin{bmatrix} 0 & -j q_z \\ j q_z & 0 \\ -j q_y & \frac{\partial}{\partial x} \end{bmatrix} \begin{bmatrix} \pi_n^x \\ \pi_n^y \end{bmatrix}. \quad (12)$$

The boundary conditions are the continuity of tangential fields (electric and magnetic) at $x = d_{1,2,\dots,(N-1)}$, as well as $A_1^{x,y} = B_N^{x,y} = 0$. This provides a system of $4(N-1)$ equations and the same number of unknowns, which can be solved numerically.

Using (4), (7), and (11), the required components of the dyadic Green's tensor for the LDOS calculations are

$$\begin{aligned} \hat{x} \cdot \overline{\overline{\mathbf{G}}}(\mathbf{r}_0, \mathbf{r}_0, \omega) \cdot \hat{x} = & \left(\frac{1}{2\pi}\right)^2 \iint_{-\infty}^{\infty} dq_y dq_z \frac{(k_0^2 \mu_m \epsilon_m + p_m^2)}{j\omega\mu_0\mu_m} \left(\frac{1}{2p_m j\omega\epsilon_0\epsilon_m} + A_m^x + B_m^x\right), \end{aligned} \quad (13)$$

$$\begin{aligned} \hat{y} \cdot \overline{\overline{\mathbf{G}}}(\mathbf{r}_0, \mathbf{r}_0, \omega) \cdot \hat{y} = & \left(\frac{1}{2\pi}\right)^2 \iint_{-\infty}^{\infty} dq_y dq_z \left\{ (B_m^x - A_m^x) \frac{q_y p_m}{\omega\mu_0\mu_m} \right. \\ & \left. + \frac{(k_0^2 \mu_m \epsilon_m - q_y^2)}{j\omega\mu_0\mu_m} \left(\frac{1}{2j\omega\epsilon_0\epsilon_m p_m} + B_m^y + A_m^y\right) \right\}. \end{aligned} \quad (14)$$

Note that we had chosen the source to be at $y = z = 0$, therefore $e^{j(q_y y + q_z z)} = 1$. It will also be helpful to use the replacement $(q_y, q_z) = (q_{\parallel} \cos\theta, q_{\parallel} \sin\theta)$ in (13) and (14),

$$\begin{aligned} \hat{x} \cdot \overline{\overline{\mathbf{G}}}(\mathbf{r}_0, \mathbf{r}_0, \omega) \cdot \hat{x} = & \frac{1}{2\pi} \int_0^{\infty} dq_{\parallel} \\ & \frac{q_{\parallel}^3}{j\omega\mu_0\mu_m} \left(\frac{1}{2j\omega\epsilon_0\epsilon_m p_m} + A_m^x + B_m^x\right), \end{aligned} \quad (15)$$

$$\begin{aligned} \hat{y} \cdot \overline{\overline{\mathbf{G}}}(\mathbf{r}_0, \mathbf{r}_0, \omega) \cdot \hat{y} = & \left(\frac{1}{2\pi}\right)^2 \int_0^{\infty} \int_0^{2\pi} d\theta dq_{\parallel} \\ & \left\{ \frac{q_{\parallel} (k_0^2 \mu_m \epsilon_m - q_{\parallel}^2 \cos^2\theta)}{j\omega\mu_0\mu_m} \left(\frac{1}{2j\omega\epsilon_0\epsilon_m p_m} + B_m^y + A_m^y\right) \right. \\ & \left. + (B_m^x - A_m^x) \frac{q_{\parallel}^2 \cos\theta p_m}{\omega\mu_0\mu_m} \right\}. \end{aligned} \quad (16)$$

Note that A_m^x and B_m^x in (15) are independent of θ due to the symmetry of the geometry for a vertical (x -directed) source. This simplifies (15) to only include a one-fold integration. Alternatively, we could obtain similar results for the vertical source by using Sommerfeld's integral form of Green's function (i.e. $\int e^{-p|x-x'|} \frac{J_0(\rho q_{\parallel})}{2p} dq_{\parallel}$). However, the spectral form of Green's function, used here, is more appropriate for a general problem with a randomly oriented source.

The integrands of (15) and (16) are the wave components departing the source with the horizontal (parallel to the boundary) wave-number of q_{\parallel} . A wave component becomes attenuating (as it travels away from the source) if $q_{\parallel} > k_0 \sqrt{\mu_m \epsilon_m}$. Such a wave component cannot carry energy away from the source unless, before its complete attenuation, it reaches a region with a supported q_{\parallel} mode (non-attenuating). Examples are when the point source is in the vicinity of an interface supporting a surface wave, or near a dielectric slab supporting a wave-guided mode.

If the dielectrics in the layered structure are lossless, i.e. ϵ_n and μ_n are real numbers, the only supported modes by the structure are Bloch modes and the wave-guided modes (confined within the layers surrounded by lower permittivity layers.) Such modes have wave-numbers smaller than $k_0 \sqrt{\mu_{\epsilon_{>}}}$, where $\mu_{\epsilon_{>}}$ is the maximum value of $\mu_n \epsilon_n$ among the layers. This means the integration limits in (15) and (16) can be truncated to $k_0 \sqrt{\mu_{\epsilon_{>}}}$,

$$\text{Im} \left\{ \hat{x} \cdot \overline{\mathbf{G}}(\mathbf{r}_0, \mathbf{r}_0, \omega) \cdot \hat{x} \right\} = \int_0^{k_0 \sqrt{\mu \varepsilon_2}} dq_{\parallel} \text{Re} \left\{ \frac{-1}{2\pi} \frac{q_{\parallel}^3}{\omega \mu_0 \mu_m} \left(\frac{1}{2j\omega \varepsilon_0 \varepsilon_m p_m} + A_m^x + B_m^x \right) \right\}, \quad (17)$$

$$\begin{aligned} \text{Im} \left\{ \hat{y} \cdot \overline{\mathbf{G}}(\mathbf{r}_0, \mathbf{r}_0, \omega) \cdot \hat{y} \right\} &= \left(\frac{1}{2\pi} \right)^2 \int_0^{k_0 \sqrt{\mu \varepsilon_2}} dq_{\parallel} \int_0^{2\pi} d\theta \text{Re} \left\{ \right. \\ &- \frac{q_{\parallel} \left(k_0^2 \mu_m \varepsilon_m - q_{\parallel}^2 \cos^2 \theta \right)}{\omega \mu_0 \mu_m} \left(\frac{1}{2j\omega \varepsilon_0 \varepsilon_m p_m} + B_m^y + A_m^y \right) \\ &\left. + (A_m^x - B_m^x) \frac{j q_{\parallel}^2 \cos \theta p_m}{\omega \mu_0 \mu_m} \right\}. \end{aligned} \quad (18)$$

As an example, consider a three layers structure consisting of a dielectric slab with $\varepsilon_1 = 11.9$ and the thickness of $T_1 = 0.3 \mu\text{m}$ immersed in a medium with $\varepsilon_2 = 2.1$. For a vertical source at the center of the slab, the integrand of (17) is shown in Fig. 2. As expected, the wave components with $q_{\parallel} < \omega \sqrt{\mu_0 \varepsilon_0 \varepsilon_2}$, which can travel in both media without attenuation, are non-zero in the integrand and contribute to the LDOS. Moreover, there is a single mode supported at $q_{\parallel} \simeq 0.75 \omega \sqrt{\mu_0 \varepsilon_0 \varepsilon_1}$ which is the guided mode inside the slab and shows up as a singularity in the integrand (a delta function). The analytical integrations of such singularities is possible using complex plane analysis and Cauchy's integration theorem. However, a simpler solution for our purpose is to add a small loss to the medium. This moves the singularity(ies) slightly away from the real axis in the complex $(\text{Re}\{q_{\parallel}\}, \text{Im}\{q_{\parallel}\})$ plane. As a result, the integrand of (17) includes a sharp peak at the singularity's q_{\parallel} . Adding more loss makes the peak broader and decreases its maximum intensity. This is in favor of the numerical calculations with the cost of becoming farther from modeling a lossless structure. Figure 2 shows the integrand for two loss values. The y-axis is truncated to clarify the broadening of the peak by increasing the loss. The same argument applies to the integrand of (18). We continue with adding $10^{-5}j$ to the permittivities throughout the rest of this paper.

Equations (2), (17), and (18), give the LDOS inside a 1D layered structure for horizontal and vertical sources. Since the calculations include two-fold integrations as well as the inversion of a $4(N-1) \times 4(N-1)$ matrix, its computational cost grows rapidly as more layers are added. However, depending on the 1D PC parameters, a finite number of layers (with manageable complexity) may suffice to model the LDOS of an infinite 1D PC. For example, in the example discussed in the next section, it turns out we only need two layers on each side of the source region in order to obtain accurate LDOS (and DOS) values in the desired frequency range.

EXAMPLE

Consider a 1D PC shown in Fig. 3 with permittivities of $\varepsilon_1 = 11.9$ (silicon), $\varepsilon_2 = 2.1$ (silicon dioxide), and thicknesses

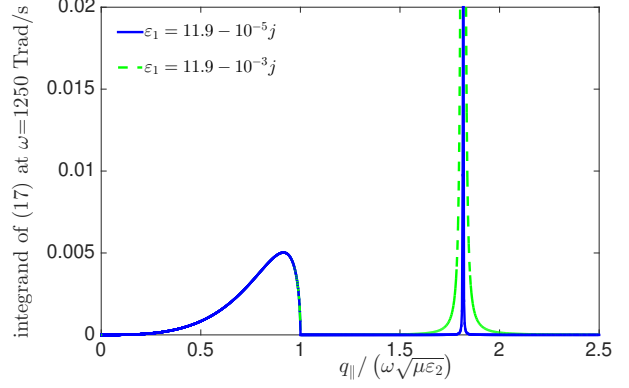


Fig. 2. The integrand of (17) for a dielectric slab with $\varepsilon_1 = 11.9$ immersed in $\varepsilon_2 = 2.1$. The vertical source with $\omega = 1250 \frac{\text{Trad}}{\text{s}}$ is located at the center of the slab. y-axis is truncated and the maximum intensities of the peaks are not shown.

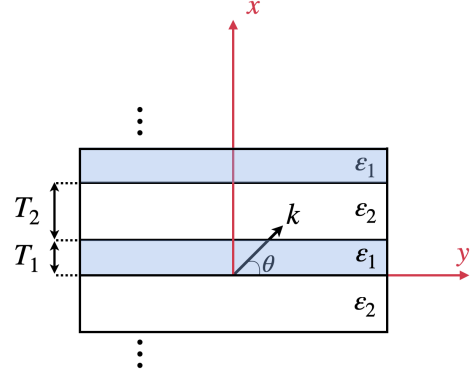


Fig. 3. The 1D PC geometry. The y- and z- dimensions are infinitely large. Parameters, in the example section, are $T_1 = 300 \text{ nm}$, $T_2 = 700 \text{ nm}$, $\varepsilon_1 = 11.9$, $\varepsilon_2 = 2.1$.

of $T_1 = 300 \text{ nm}$, $T_2 = 700 \text{ nm}$. Consider a vertical (w.r.t. the layers boundaries) point source located at the center of the ε_2 region. We approximate this geometry with a finite number of layers around the source region similar to Fig. 1, and examine the LDOS by increasing the number of layers.

Figure 4 shows the integrand of 17 for a layered structure with five, seven, and nine layers, and parameters similar to Fig. 1. The vertical (x-directed) source is at the center of the ε_1 region. The nine layers geometry is also shown in Fig. 4 as a reference. By removing one and two of the outermost layers from each side of this geometry, the seven and five layers geometries are obtained, respectively. As Fig. 4 shows, the integrands of the three geometries have the sharp peak associated with the wave-guided mode with the same $q_{\parallel} \simeq 0.75 \omega \sqrt{\mu_0 \varepsilon_0 \varepsilon_1}$ (and the same intensity, which is not shown in Fig. 4). Other non-zero values of the integrand are associated with the propagating modes which essentially become Bloch modes as the number of layers increases sufficiently.

Fig. 5 shows the calculated LDOS of the layered structures using (2) and (17). Fig. 5 also includes the local density of propagating states ($\text{LDOS}_{\text{propagating}}$) by removing the wave-guided mode's contribution to the LDOS. This quantity should merge to the local density of Bloch states, $\text{LDOS}_{\text{Bloch}}$,

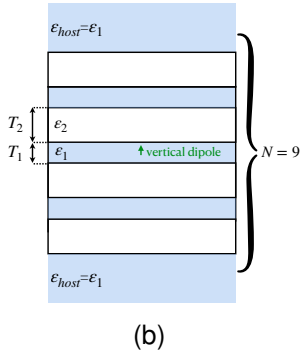
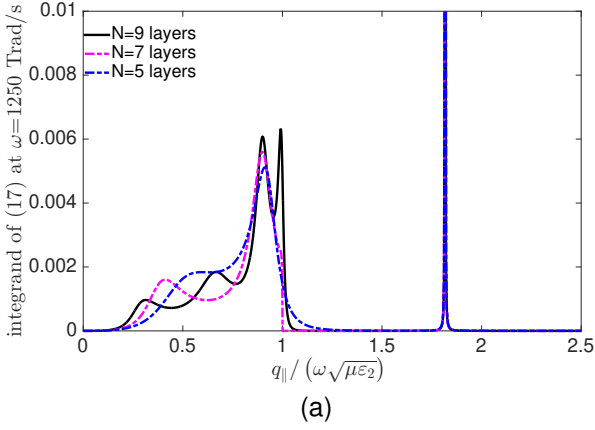


Fig. 4. a) the integrand of (17) for a vertical source at the center of the ϵ_1 region in Fig. 3 geometry modeled with a finite number of layers, (b) the nine layers model as a reference. Removing one and two of the outermost layer from each side gives the seven and five layers models, respectively.

as the number of layers grows sufficiently. It can be seen that the LDOS of the five layers geometry does not change noticeably above $\omega = 250 \text{ Trad/s}$ by adding more layers. This is mostly because the wave-guided mode's contribution dominates propagating modes' contribution to the LDOS. As a result, we may use the five layers geometry to study the LDOS and DOS of the infinite 1D PC shown in Fig. 3. However, approximating Bloch mode densities of the 1D PC based on the $\text{LDOS}_{\text{propagating}}$ of the five layers geometry will have a limited accuracy, as Fig. 4 (b) shows. We will discuss this issue, along with a solution later. The same conclusions hold with a different source location and orientation. In the following, we continue with the five layers model, and compare the calculated LDOS and $\text{LDOS}_{\text{propagating}}$ with alternative methods.

Figure 6 shows the LDOS of the 1D PC for both horizontal and vertical sources as a function of the source location and radial frequency. Depending on the frequency, LDOS in the higher permittivity region may become smaller than the lower permittivity region. This will not be surprising if we consider that, beside the number of available modes, the source-mode coupling intensity is involved in the LDOS calculations. The larger LDOS at the edges of the ϵ_1 region at $\omega = 1250 \text{ Trad/s}$ is consistent with the scalar calculations in [36].

As discussed earlier, the LDOS in a 1D PC is due to both Bloch modes propagation carrying energy away from the source as well as the guided modes confined mostly within the

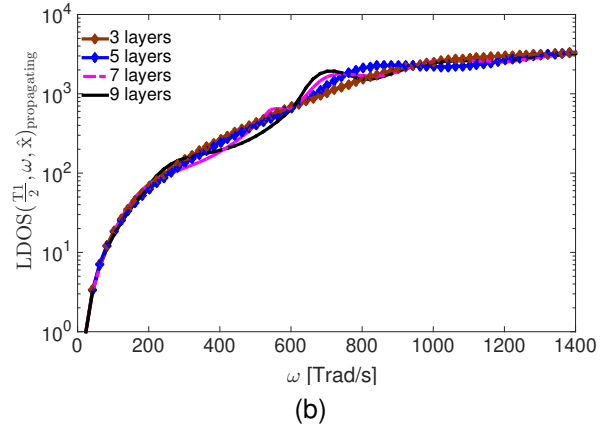
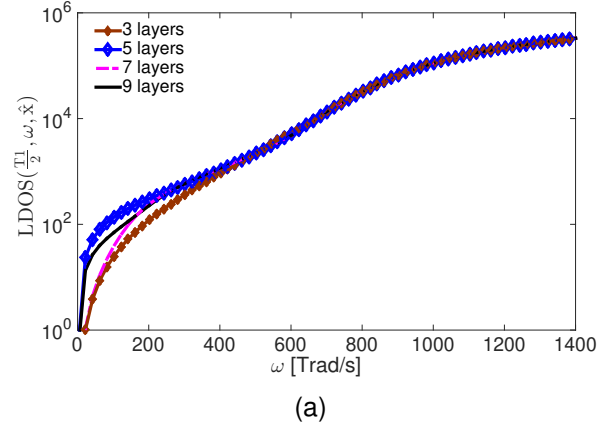


Fig. 5. The LDOS (a) and $\text{LDOS}_{\text{propagating}}$ (b) inside 3 geometry modeled with different number of layers. The source is vertical and at the center of the middle ϵ_1 region.

ϵ_2 region which do not leave the structure (in case of a finite size in x - dimension) [24]. The contribution of these guided modes to the LDOS can be subtracted by removing the singularities of the Green's tensor's integrand (we call this quantity $\text{LDOS}_{\text{propagating}}$). Figure 7 shows the $\text{LDOS}_{\text{propagating}}$ of the five layers geometry. Later we compare this quantity with the Bloch density of the infinite 1D PC. Comparison between Fig. 6 and Fig. 7 confirms that the guided modes are the dominant contributors to the LDOS, especially in the layers with the higher permittivity. As a clarification, Fig. 7 also includes a comparison between the LDOSs with and without including the guided modes at $\omega = 1250 \text{ Trad/s}$. As expected, the guided modes' contribution to the LDOS becomes minimized in the central locations of the lower permittivity layer.

Figure 8 (a) shows the calculated DOS and $\text{DOS}_{\text{propagating}}$ of the layered geometry using (6). It also includes DOS of isotropic homogeneous media with permittivities of 2.1 and 11.9, as a reference. These DOSs are the estimated values for an infinite 1D PC based on the five layered structure calculations. As discussed earlier, the LDOS and DOS calculations of the five layered structure (at $\omega > 250 \frac{\text{Trad}}{\text{s}}$) are very close to an infinite 1D PC with the same material properties (Fig. 5(a)). This was because these quantities are mainly determined by the guided modes within the higher permittivity layers.

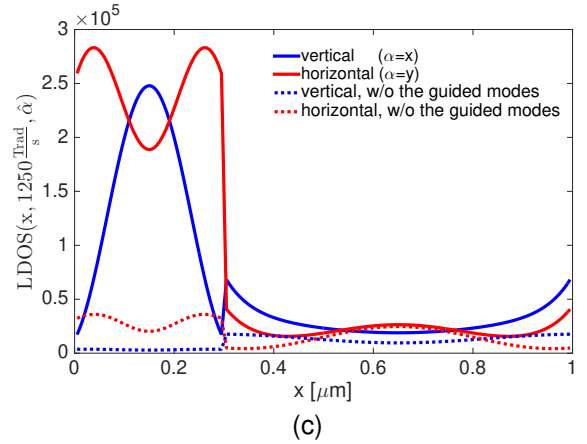
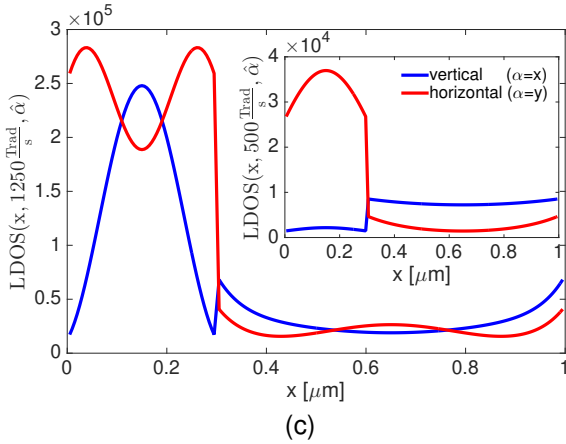
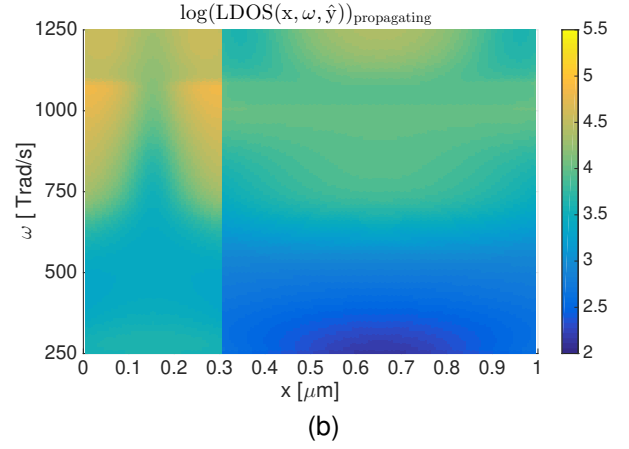
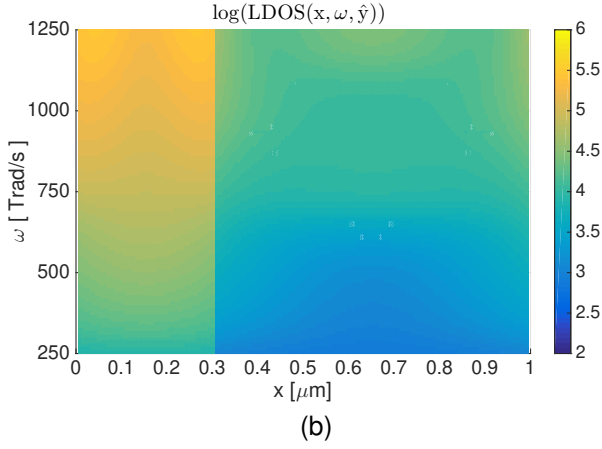
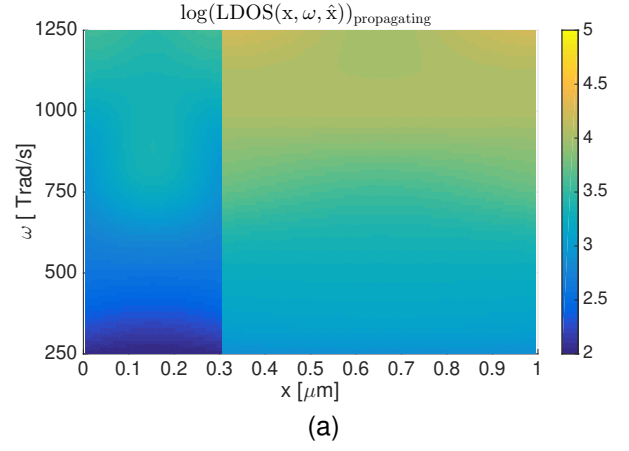
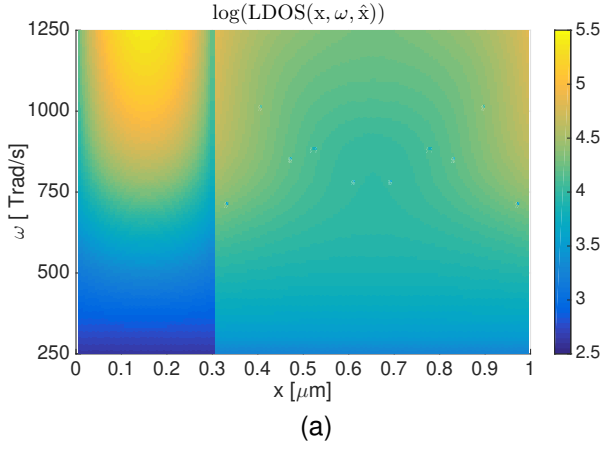


Fig. 6. The LDOS of the 1D PC shown in Fig. 3 for a vertical source (a), a horizontal source (b), and at $\omega = 500, 1250 \text{ Trad/s}$ (c).

Fig. 7. The $\text{LDOS}_{\text{propagating}}$ of the five layer geometry for a vertical source (a) and a horizontal source (b). (c) is the LDOS with and without the guided modes at $\omega = 1250 \text{ Trad/S}$.

However, as Fig. 5(b) showed, using $\text{DOS}_{\text{propagating}}$ of the five layers structure to approximate $\text{DOS}_{\text{Bloch}}$ of the 1D PC has limited accuracy and needed to be studied. To do so, we calculate $\text{DOS}_{\text{Bloch}}$ of the infinite 1D PC using its dispersion relations [Archived document]. A non-magnetic 1D PC as shown in Fig. 3, has Bloch modes dispersion relations as [22], [37]

$$\begin{aligned} \cos((T_1 + T_2)k_x) &= \cos(k_{x1}T_1) \cos(k_{x2}T_2) \\ &\quad - 0.5 \left(\frac{p_2}{p_1} + \frac{p_1}{p_2} \right) \sin(k_{x2}d_2) \sin(k_{x1}d_1), \end{aligned} \quad (19)$$

where

$$k_{xi} = \sqrt{k_i^2 - k_y^2 - k_z^2}, \quad p_i = \begin{cases} \frac{k_{xi}}{\omega\mu_0} & TE \\ \frac{\omega\varepsilon_0\varepsilon_i}{k_{xi}} & TM \end{cases}, \quad (20)$$

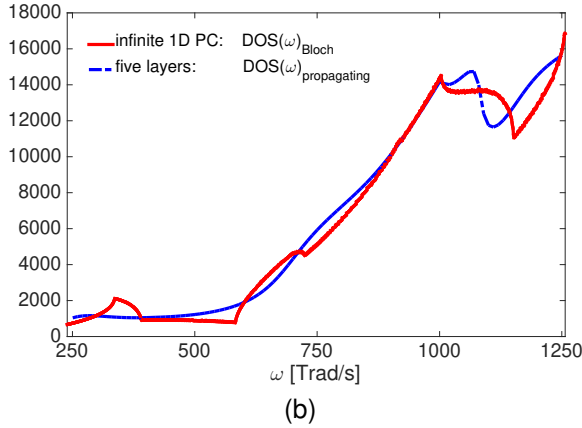
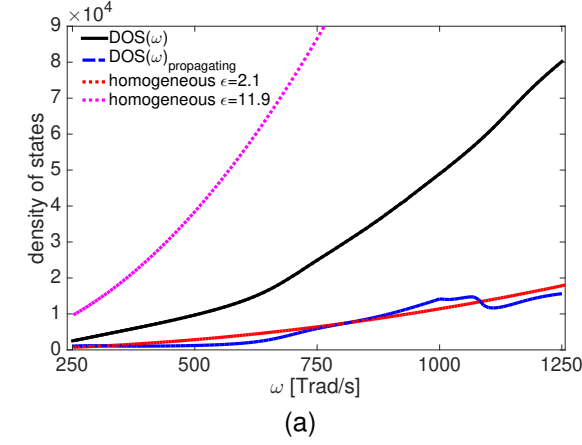


Fig. 8. (a) the DOS and $\text{DOS}_{\text{propagating}}$ of the 1D PC shown in Fig. 3 using the five layers model, (b) comparison between $\text{DOS}_{\text{propagating}}$ (of the five layers model) and $\text{DOS}_{\text{Bloch}}$ (of an infinite 1D PC).

and transverse electric (TE) and magnetic (TM) modes are defined with respect to the y - z plane (interface plane). The Bloch density of states can be calculated as

$$\text{DOS}_{\text{Bloch}}(\omega) = \sum_{j=TE, TM} \frac{\omega \varepsilon_2}{4c^2 \pi^2} \int_0^\pi d\theta \left| \left(\cos\theta \frac{\partial k_x^j(\omega, \theta)}{\partial \theta} + \omega \sin\theta \frac{\partial k_x^j(\omega, \theta)}{\partial \omega} \right) \cos\theta \right|. \quad (21)$$

where $\varepsilon_2 < \varepsilon_1$.

Figure 8(b) shows the comparison between $\text{DOS}_{\text{Bloch}}$ of an infinite 1D PC (using (21)) and $\text{DOS}_{\text{propagating}}$ of the five layers geometry. Although the two quantities remain close in the entire frequency interval, $\text{DOS}_{\text{propagating}}$ misses some of the derivative discontinuities in $\text{DOS}_{\text{Bloch}}$. Figure 8(b) also reveals the amount of inaccuracy that presents in the total DOS calculation (black curve in Fig. 8(a)). In fact, we can remove such inaccuracy by replacing $\text{DOS}_{\text{propagating}}$ contribution in the total DOS calculation with $\text{DOS}_{\text{Bloch}}$. This is not shown in figures, as the change was not noticeable (since the DOS is dominated by the guided modes).

FEM VERIFICATION AND COMPARING (2) WITH (5)

In order to verify the LDOS calculations, the 1D PC structure is numerically solved using a full-wave solver based on FEM [38] and the results are compared in Figs. 9 and 10. In the FEM modeler, a small cylinder with the surface area of δs is placed at the source location (we used height and perimeter of 10 nm) with its axis aligned to $\hat{\alpha}$ direction. A surface electric/magnetic current (J_α^e/J_α^m) is enforced on the surface of the cylinder, directed along its axis. The real part of the electric/magnetic field component co-directed with the applied current is averaged over the cylinder volume and is extracted ($\text{Re}\{E_\alpha^{\text{ave}}\}/\text{Re}\{H_\alpha^{\text{ave}}\}$). The necessary components of the Green's tensors for the LDOS calculations are simply

$$\begin{aligned} \left| \omega \mu_0 \mu_r \text{Im} \left(\hat{\alpha} \cdot \overline{\overline{\mathbf{G}}}_{\mathbf{E}}(\mathbf{r}_0, \mathbf{r}_0, \omega) \cdot \hat{\alpha} \right) \right| &= \left| \frac{\text{Re}\{E_\alpha^{\text{ave}}\}}{J_\alpha^e \delta s} \right| \\ \left| \omega \varepsilon_0 \varepsilon_r \text{Im} \left(\hat{\alpha} \cdot \overline{\overline{\mathbf{G}}}_{\mathbf{H}}(\mathbf{r}_0, \mathbf{r}_0, \omega) \cdot \hat{\alpha} \right) \right| &= \left| \frac{\text{Re}\{H_\alpha^{\text{ave}}\}}{J_\alpha^m \delta s} \right|. \end{aligned} \quad (22)$$

The lateral dimensions of the structure is truncated to 1.25λ , and perfect matched layer (PML) are used as the boundary conditions. Increasing the number of layers beyond five, or the lateral dimensions of the geometry does not change the calculated LDOSs noticeably, which ensures the convergence of the calculations. Figures 9 and 10 show good agreement between the theoretical calculations and the FEM results.

As mentioned earlier, the LDOS calculations in this paper were based on the electric point source only, i.e. (2), with the implicit assumption that the contributions of the electric and magnetic point sources to the LDOS are equal. As discussed in details in [4], in a general medium (e.g. anisotropic), (2) is an approximation, and (5) is the accurate LDOS expression. As a comparison, Fig. 11(a) shows the LDOS calculations based on the electric and magnetic point sources (vertical and horizontal orientations) at the center of the ε_1 region. It is clear that the 1D PC LDOS calculations based on (2) and (5) have differences as the electric and magnetic dipoles' couplings to the available modes, at a specific location, are generally different. However, as Fig. 11 shows, the average LDOS in all directions is less dependent on the considered point sources. The calculated DOS based on (2) is almost as accurate as using (5). Accurate calculation of the LDOS based on (5), although follows a similar procedure, is beyond the scope of this document.

To briefly discuss the application of the obtained results in the context of thermal radiation, consider a 1D PC as the emitting body. The DOS for the emitters deep inside the 1D PC, as apparent from Fig. 8, is not exactly proportional to ω^2 . However, the $\text{DOS}_{\text{Bloch}}$ is the more relevant quantity in thermal studies rather than the total DOS since the photons in the guided modes cannot leave the 1D PC. The $\text{DOS}_{\text{Bloch}}$ in Fig. 8 proves that emission from a 1D PC can have a non-Planckian distribution (note that Planckian distribution is a result of ω^2 dependence of the DOS). However, the obtained results are not conclusive about whether the emission can surpass the Planck's limit because of the reflection at the surface of a finite-size 1D PC. In order to find the surface reflection impact, we can find the electric (far) field in the

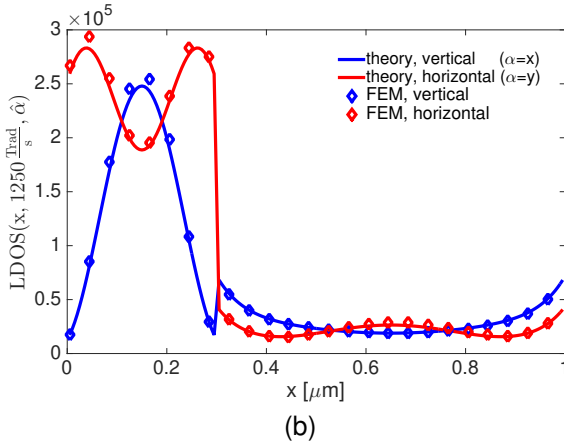
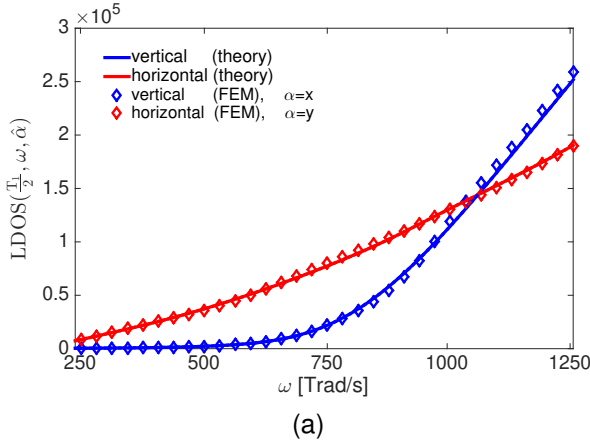


Fig. 9. Theoretical calculation of the LDOS versus the full-wave solver results based on FEM at the center of the ε_1 region (a) and at $\omega = 1250 \frac{\text{Trad}}{\text{s}}$ (b).

outer most layer (i.e. layer N in Fig. 1) generated by a point source inside the layered structure using (9) to (12). The ratio of the emitted power into the outer half-space to the total power departing the point source is the quantity which can approximate the surface reflection impact, and determines whether the radiations to the outer space can exceed Planck's limit. This is a subject for a follow up study.

CONCLUSION

The formulations were provided for the exact LDOS calculations inside a layered structure based on its Green's tensor. The relations were used to calculate LDOS, DOS, and $\text{DOS}_{\text{Bloch}}$ of a 1D PC. Using parameters of a practical 1D PC at visible range, the quantities were calculated for a five layer structure. It was shown that LDOS and DOS of the 1D PC can be well-approximated by the five layers geometry above a certain frequency. The exact $\text{DOS}_{\text{Bloch}}$ inside an infinite 1D PC was also calculated based on its dispersion relations, and was compared with the approximation by the five layers geometry. The results were also verified with a wave-solver based on FEM. The calculated $\text{DOS}_{\text{Bloch}}$ inside the 1D PC verifies the non-Planckian thermal emission inside a 1D PC.

REFERENCES

- [1] G. Kirchhoff, "ueber das verhältniss zwischen dem emmissionsvermögen und dem absorptionsvermögen der körper für wärme and licht," *annalen*

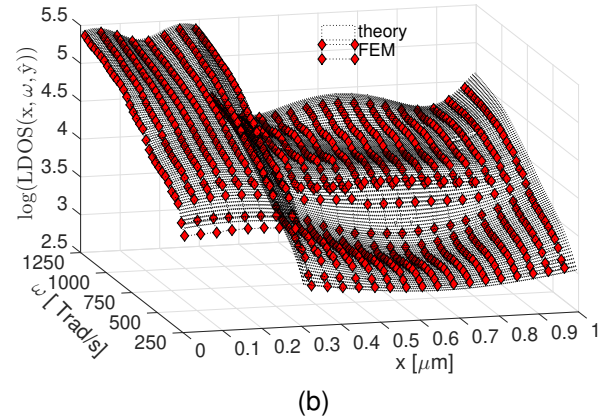
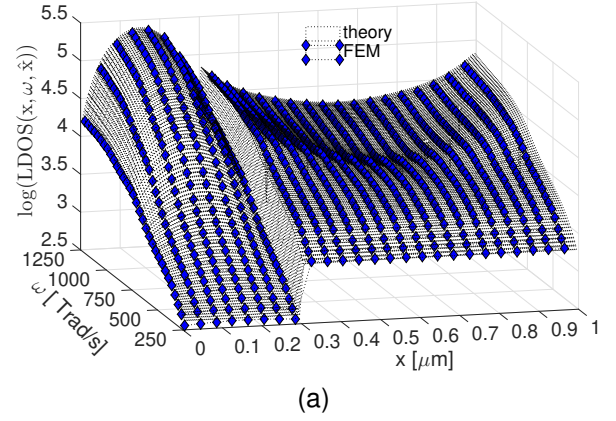


Fig. 10. Theoretical calculation of the LDOS versus the full-wave solver results based on FEM as a function of radial frequency and location for a vertical (a) and horizontal emitter (b).

- der physik und chemie 109 (2), 275–301 (1860). "on the relation between the radiating and absorbing powers of different bodies for light and heat," *Philosophical Magazine and Journal of Science, Series 4, Vol.*, vol. 20, pp. 1–21, 1860.
- [2] M. Planck, *The theory of heat radiation*. Courier Corporation, 2013.
- [3] E. N. Economou, *Green's functions in quantum physics*. Springer Science & Business Media, 2006, vol. 7.
- [4] K. Joulain, R. Carminati, J.-P. Mulet, and J.-J. Greffet, "Definition and measurement of the local density of electromagnetic states close to an interface," *Physical Review B*, vol. 68, no. 24, p. 245405, 2003.
- [5] P. Lodahl, S. Mahmoodian, and S. Stobbe, "Interfacing single photons and single quantum dots with photonic nanostructures," *Reviews of Modern Physics*, vol. 87, no. 2, p. 347, 2015.
- [6] W. Li and S. Fan, "Nanophotonic control of thermal radiation for energy applications," *Optics express*, vol. 26, no. 12, pp. 15 995–16 021, 2018.
- [7] M.-L. Hsieh, S.-Y. Lin, J. A. Bur, and R. Shenoi, "Experimental observation of anomalous thermal radiation from a three-dimensional metallic photonic crystal," *Nanotechnology*, vol. 26, no. 23, p. 234002, 2015.
- [8] D. Englund, D. Fattal, E. Waks, G. Solomon, B. Zhang, T. Nakaoka, Y. Arakawa, Y. Yamamoto, and J. Vučković, "Controlling the spontaneous emission rate of single quantum dots in a two-dimensional photonic crystal," *Physical review letters*, vol. 95, no. 1, p. 013904, 2005.
- [9] J. D. Joannopoulos, P. R. Villeneuve, and S. Fan, "Photonic crystals," *Solid State Communications*, vol. 102, no. 2-3, pp. 165–173, 1997.
- [10] D. Kleppner, "Inhibited spontaneous emission," *Physical review letters*, vol. 47, no. 4, p. 233, 1981.
- [11] A. S. Sanchez and P. Halevi, "Spontaneous emission in one-dimensional photonic crystals," *Physical Review E*, vol. 72, no. 5, p. 056609, 2005.
- [12] E. Yablonovitch, "Photonic crystals," *Journal of Modern Optics*, vol. 41, no. 2, pp. 173–194, 1994.

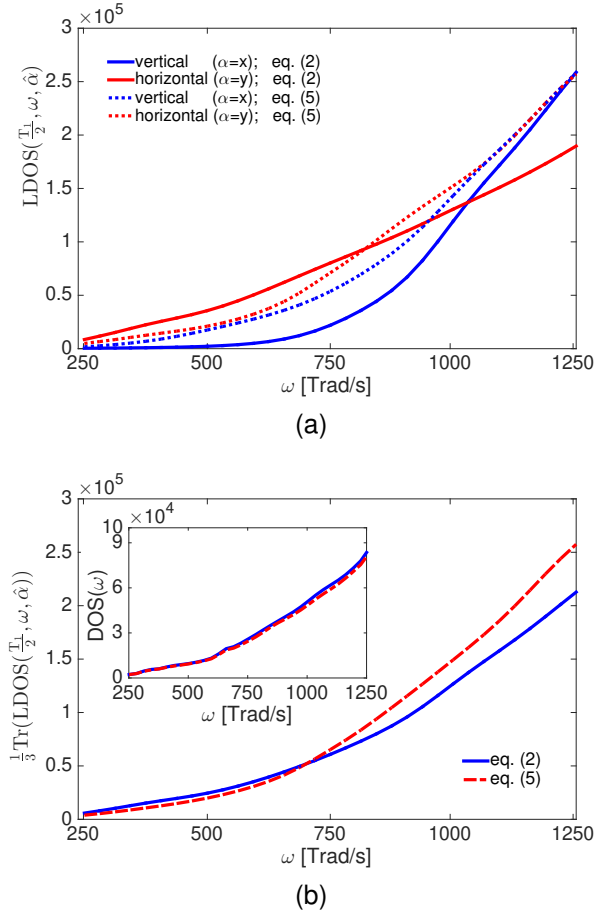


Fig. 11. (a) the LDOS of the 1D PC at the center of the ε_2 region using (2) and (5). (b) the average LDOS in all directions at the center of the ε_1 region, and the DOS (insert) using (2) and (5).

[13] S. B. Hasan, A. P. Mosk, W. L. Vos, and A. Lagendijk, "Finite-size scaling of the density of states in photonic band gap crystals," *Physical review letters*, vol. 120, no. 23, p. 237402, 2018.

[14] W. W. Chow, "Theory of emission from an active photonic lattice," *Physical Review A*, vol. 73, no. 1, p. 013821, 2006.

[15] C. M. Cornelius and J. P. Dowling, "Modification of planck blackbody radiation by photonic band-gap structures," *Physical Review A*, vol. 59, no. 6, p. 4736, 1999.

[16] D. Thompson, L. Zhu, R. Mittapally, S. Sadat, Z. Xing, P. McArdle, M. M. Qazilbash, P. Reddy, and E. Meyhofer, "Hundred-fold enhancement in far-field radiative heat transfer over the blackbody limit," *Nature*, vol. 561, no. 7722, pp. 216–221, 2018.

[17] S.-Y. Lin, M.-L. Hsieh, S. John, B. Frey, J. A. Bur, T.-S. Luk, X. Wang, and S. Narayanan, "An in-situ and direct confirmation of super-planckian thermal radiation emitted from a metallic photonic-crystal at optical wavelengths," *Scientific reports*, vol. 10, no. 1, pp. 1–7, 2020.

[18] S. John and R. Wang, "Metallic photonic-band-gap filament architectures for optimized incandescent lighting," *Physical Review A*, vol. 78, no. 4, p. 043809, 2008.

[19] C. Luo, A. Narayanaswamy, G. Chen, and J. Joannopoulos, "Thermal radiation from photonic crystals: a direct calculation," *Physical Review Letters*, vol. 93, no. 21, p. 213905, 2004.

[20] G. Boedeker and C. Henkel, "All-frequency effective medium theory of a photonic crystal," *Optics Express*, vol. 11, no. 13, pp. 1590–1595, 2003.

[21] E. Yeganegi, A. Lagendijk, A. P. Mosk, and W. L. Vos, "Local density of optical states in the band gap of a finite one-dimensional photonic crystal," *Physical Review B*, vol. 89, no. 4, p. 045123, 2014.

[22] J. Joannopoulos, R. Meade, and J. Winn, "Photonic crystals," *Molding the flow of light*, 1995.

[23] V. Prosentsov and A. Lagendijk, "The local density of states in finite size photonic structures, small particles approach," *Photonics and*

Nanostructures-Fundamentals and Applications, vol. 5, no. 4, pp. 189–199, 2007.

[24] M. Wubs and A. Lagendijk, "Local optical density of states in finite crystals of plane scatterers," *Physical Review E*, vol. 65, no. 4, p. 046612, 2002.

[25] M. Wubs, L. Suttrop, and A. Lagendijk, "Spontaneous-emission rates in finite photonic crystals of plane scatterers," *Physical Review E*, vol. 69, no. 1, p. 016616, 2004.

[26] S. Brueck, V. Smagley, and P. Eliseev, "Radiation from a dipole embedded in a multilayer slab," *Physical Review E*, vol. 68, no. 3, p. 036608, 2003.

[27] S. Brueck, "Radiation from a dipole embedded in a dielectric slab," *IEEE Journal of Selected Topics in Quantum Electronics*, vol. 6, no. 6, pp. 899–910, 2000.

[28] A. Sommerfeld, *Partial differential equations in physics*. Academic press, 1949.

[29] R. Moore and W. Blair, "Dipole radiation in a conducting half-space," *J. Res. NBS*, vol. 65, no. 6, pp. 547–563, 1961.

[30] H. Hoekstra and H. Elrofai, "Theory of optical spontaneous emission rates in layered structures," *Physical Review E*, vol. 71, no. 4, p. 046609, 2005.

[31] G. W. Hanson and A. B. Yakovlev, *Operator theory for electromagnetics: an introduction*. Springer Science & Business Media, 2013.

[32] G. Hanson, A. Nosich, and E. Kartchevski, "Green's function expansions in dyadic root functions for shielded layered waveguides," *Progress In Electromagnetics Research*, vol. 39, pp. 61–91, 2003.

[33] G. W. Hanson, A. B. Yakovlev, and J. Hao, "Leaky-wave analysis of transient fields due to sources in planarly layered media," *IEEE Transactions on Antennas and Propagation*, vol. 51, no. 2, pp. 146–159, 2003.

[34] A. B. Yakovlev and G. W. Hanson, "Fundamental modal phenomena on isotropic and anisotropic planar slab dielectric waveguides," *IEEE Transactions on Antennas and Propagation*, vol. 51, no. 4, pp. 888–897, 2003.

[35] J. Bagby and D. Nyquist, "Dyadic green's functions for integrated electronic and optical circuits," *IEEE transactions on microwave theory and techniques*, vol. 35, no. 2, pp. 207–210, 1987.

[36] A. Moroz, "Minima and maxima of the local density of states for one-dimensional periodic systems," *EPL (Europhysics Letters)*, vol. 46, no. 4, p. 419, 1999.

[37] L. Qi and C. Liu, "Complex band structures of 1d anisotropic graphene photonic crystal," *Photonics Research*, vol. 5, no. 6, pp. 543–551, 2017.

[38] *COMSOL Multiphysics*, www.comsol.com, Stockholm, Sweden, 2021.